Direct Lyapunov exponent analysis enables parametric study of transient signalling governing cell behaviour

B.B. Aldridge, G. Haller, P.K. Sorger and D.A. Lauffenburger

Abstract: Computational models aid in the quantitative understanding of cell signalling networks. One important goal is to ascertain how multiple network components work together to govern cellular responses, that is, to determine cell 'signal-response' relationships. Several methods exist to study steady-state signals in the context of differential equation-based models. However, many biological networks influence cell behaviour through time-varying signals operating during a transient activated state that ultimately returns to a basal steady-state. A computational approach adapted from dynamical systems analysis to discern how diverse transient signals relate to alternative cell fates is described. Direct finite-time Lyapunov exponents (DLEs) are employed to identify phase-space domains of high sensitivity to initial conditions. These domains delineate regions exhibiting qualitatively different transient activities that would be indistinguishable using steady-state analysis but which correspond to different outcomes. These methods are applied to a physicochemical model of molecular interactions among caspase-3, caspase-8 and X-linked inhibitor of apoptosis – proteins whose transient activation determines cell death against survival fates. DLE analysis enabled identification of a separatrix that quantitatively characterises network behaviour by defining initial conditions leading to apoptotic cell death. It is anticipated that DLE analysis will facilitate theoretical investigation of phenotypic outcomes in larger models of signalling networks.

1 Introduction

Reaction models employing differential equations are frequently used as tools for computational exploration of complex biomolecular networks, such as those involved in signal transduction of extracellular stimuli governing cell fate. These models, generally based on mass-action kinetics, incorporate network topology and quantitatively describe the kinetics of interactions between network components [1–8]. Because these mechanistic models are large and complicated, quantitative analysis is necessary to extract understanding [6, 9]. A typical objective of model analysis is to comprehensively characterise the response of the signalling network to changes in system parameters. By altering network behaviour, changes to protein levels or reaction rates may lead to different cell fates following exogenous stimulation [10–13]. As an example, activation of the small GTP-binding protein Ras can induce a variety of cell responses including cell proliferation and differentiation, depending on the cell type and extracellular conditions. Perturbations to the Ras-mediated regulatory network can promote pathological cell behaviour; mutations that affect Ras levels or binding or reaction rates are often linked to cancer [14]. Numerous similar examples may be found underlying cell behavioural dysregulation; thus, illuminating how changes in molecular interactions alter signalling network behaviour is key to understanding the molecular basis of disease. Simulations can be used to inspect signalling behaviour arising from network perturbations of potential interest – perhaps a genetic mutation or pharmacological intervention [6, 15]. By simulating a mechanistic model, predictions can be made about how specific changes to parameters such as stimulation or drug inhibition conditions, initial concentrations and reaction rates will affect signalling [4, 16–21]. To link different cell responses to complex signalling interactions, however, more systematic, comprehensive analysis methods need to be applied.

Common systematic tools for studying the behaviour of differential equation models for signalling networks include parameter sensitivity analysis and steady-state analysis. Determining sensitivity to rate constants and initial conditions (i.e. protein levels at the initial time point) is useful for finding reactions and species that are particularly important in the overall reaction scheme [22–24]. However, the local sensitivities that may arise from intertwined multivariate interactions cannot be revealed by single-parameter sensitivity analysis. A comprehensive analysis, where several parameters are changed simultaneously, is often computationally impractical and the results intractable. The analysis method presented in this work is based on direct Lyapunov exponents (DLEs), which is a comprehensive local sensitivity analysis of model initial conditions. The DLE approach can be interpreted in a manner that is analogous to steady-state analysis of metabolic networks. Our analysis goal is to understand

IEE Proceedings online no. 20050065

doi:10.1049/ip-syb:20050065

Paper first received 13th September 2005 and in revised form 3rd May 2006

B.B. Aldridge, P.K. Sorger and D.A. Lauffenburger are with the Biological Engineering Division, and with the Center for Cell Decision Processes, MIT, Cambridge, MA 02139, USA

G. Haller is with the Department of Mechanical Engineering, MIT, Cambridge, MA 02139, USA

E-mail: breea@mit.edu

how the qualitative network behaviour (the biological fate) depends on the quantitative combinations of network component parameters (the network state).

Steady-state analysis methods have been established in dynamical systems as powerful methods for analysing models of a variety of physico-chemical processes, including fluid flow and chemical reactions. These techniques, including fixed-point bifurcation methods, have been successfully used to study several biological network models. These methods delineate how changes in initial conditions and rate parameters affect the biological outcomes associated with different equilibria. Good candidates for this analysis are systems with multiple steady-states, where each phenotypic behaviour is associated with a particular steady-state. Examples include metabolic networks, the cell cycle and engineered gene networks [2, 5, 25–27]. In contrast, many signal transduction networks affect cell fate through transient, pre-steady-state signals. Here, we will refer to these systems as 'transient response networks'. In transient response networks, rapidly changing signals, or transients, other signals that propagate through the pathways [10, 19, 20, 28]. In these systems, the time evolution of transient signals, not steady-state signals, influences cell behaviour. For this reason, transient response systems may not be good candidates for steady-state analysis. To understand these systems, we require methods that analyse transient signals, such as DLE analysis described here.

The transient response system that we analyse in this work is a core sub-network of the signal transduction cascade regulating the programmed cell death (apoptosis)-against-survival phenotypic decision. Apoptosis has in some previous work been modelled as a bistable system where death and survival are distinct stable steady-states [29, 30]. However, this is not the only way, nor necessarily the most appropriate way, to cast a problem that appears to involve a transient response network [10, 28, 31]. In fact, models focusing on the later stages of the apoptotic decision such as ours as well as one of the alternative models developed by Eissing *et al.* [29] do not exhibit bistablity. In response to apoptotic stimuli, this network produces a transient response that is dependent on the stimuli and the state of the cell. The transient signals will either lead to apoptosis (where the network does not reset because the cell dies) or survival (where the network resets).

Apoptosis is induced by extrinsic (receptor-dependent) and intrinsic (intracellular) pathways. Common to both pathways is the activation of caspases, a family of proteases that execute the cell death decision by cleaving protein targets. The caspases activate each other to form a protease cascade and are themselves subject to regulation by many other proteins [32–34]. Caspases are synthesised in an inactive state (pro-caspases or zymogens) and become active when dimerised or cleaved by other caspases. Intracellular or extracellular pro-death stimuli lead to dimerisation and cleavage of initiator caspases such as caspase-8. Once activated, these initiator caspases in turn cleave and activate effector caspases such as caspase-3 (Fig. 1). Activation of initiator by effector caspases generates positive feedback that can amplify this cascade [32, 35]. Prolonged activation of effector caspases leads to programmed cell death. A critical inhibitor is X-linked inhibitor of apoptosis (XIAP), which negatively regulates the enzymatic activity of caspase-3. Additionally, XIAP tags active caspase-3 for ubiquitination. This modification promotes caspase-3 degradation and causes caspase-3 activity to be transient [36, 37].

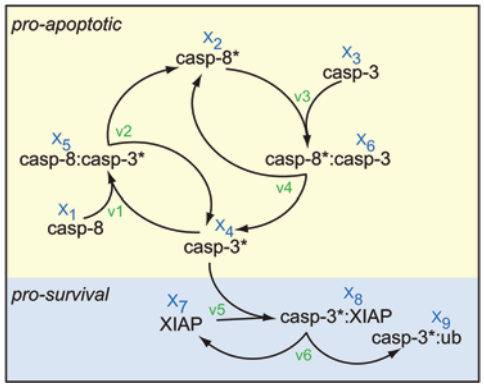

Fig. 1 *Schematic of mathematical model for caspase-3 activation*

Caspase-3 (casp-3) activity is regulated by caspase-8 (casp-8) and XIAP. Caspase-8 (an initiator caspase) activates caspase-3 (an effector caspase) after forming a complex. Positive feedback is similarly accomplished through activation of caspase-8 by caspase-3. XIAP inhibits active caspase-3 by tagging it for ubiquitination and degradation. Here, a star indicates the active form of the caspases, a colon indicates a complex, and 'ub' indicates ubiquitination tagging. Labels in X and v series correspond with species and reaction numbers, respectively

Analogous to the application of steady-state analyses to signalling networks where equilibria correspond to cell response, we describe direct finite-time Lyapunov exponent (DLE) analysis as a method to study transient response signalling networks. We use DLEs to analyse how transient signalling dynamics are affected as different parameters change individually or simultaneously in multi-dimensional phase space (the set of initial chemical species concentrations). DLE analysis is not the first method to measure local sensitivity analysis, but is distinguished from previously applied techniques because DLEs are calculated as parameters change simultaneously, not individually [23]. DLEs were originally used to find invariant manifolds in dynamical systems and fluid flows [38–41]. Similarly, we use DLEs to find separatrices, or sensitive regions in phase space that separate signals giving rise to different responses. Separatrices are useful because they quantitatively identify points at which continuous change in species concentration lead to dramatic, discontinuous change in response. As an example of current interest in molecular cell biology, we used DLEs to analyse a small, mechanistic model of a transient response network describing caspase-3 activation in the network described above. We were able to characterise initial conditions (concentrations of protein species) leading to survival and apoptosis with the DLE-defined separatrix, but not by examining steady-states. We thereby gained conceptual insight into the integrated effects of multiple components in this network.

2 Methods

2.1 Caspase-3 activation model

A system of ordinary differential equations describing the activation of caspase-3 by caspase-8 was constructed using mass-action kinetics and the known topology of this portion of the apoptosis regulatory network (Fig. 1). We have made the following central assumptions: (a) chemical species are present at spatially-uniform concentrations; (b) caspase-6 is not involved in the feedback between active caspase-3 and caspase-8; (c) ubiquitination can be represented by a single lumped reaction; and (d) caspase

activation is achieved after an inactive caspase interacts with an active caspase. The differential equation describing the concentration of active caspase-3 tagged for ubiquitination (x_9) was removed from the model because it does affect the network. Values for the rate constants are listed in Table 1. The equations defining the model are as follows:

$$\dot{x}_1 = -k_1 x_4 x_1 + k_{d1} x_5 \quad (1)$$

$$\dot{x}_2 = k_{d2} x_5 - k_3 x_2 x_3 + k_{d3} x_6 + k_{d4} x_6 \quad (2)$$

$$\dot{x}_3 = -k_3 x_2 x_3 + k_{d3} x_6 \quad (3)$$

$$\dot{x}_4 = k_{d4} x_6 - k_1 x_4 x_1 + k_{d1} x_5 - k_5 x_7 x_4 + k_{d5} x_8 + k_{d2} x_5 \quad (4)$$

$$\dot{x}_5 = -k_{d2} x_5 + k_1 x_4 x_1 - k_{d1} x_5 \quad (5)$$

$$\dot{x}_6 = -k_{d4} x_6 + k_3 x_2 x_3 - k_{d3} x_6 \quad (6)$$

$$\dot{x}_7 = -k_5 x_7 x_4 + k_{d5} x_8 + k_{d6} x_8 \quad (7)$$

$$\dot{x}_8 = k_5 x_7 x_4 - k_{d5} x_8 - k_{d6} x_8 \quad (8)$$

2.2 Direct finite-time Lyapunov exponent

The DLE is a measure of local sensitivity to changes in initial conditions, evaluated multi-dimensionally at a finite-time, as depicted for one dimension in Fig. 2. First, for a selected trajectory, the derivative of the current trajectory position with respect to its initial location is calculated in all independent directions at each finite-time instant of interest. These directional derivatives are in turn assembled into a time-dependent gradient matrix, whose entries are indicative of the rate at which neighbouring trajectories separate in the corresponding directions. The spectral norm (or largest singular value) of the gradient matrix gives the instantaneous maximal rate of local trajectory separation over all directions. The DLE associated with the selected trajectory is then defined as the time-averaged logarithm of the above norm, measuring the maximal rate of exponential separation between the underlying trajectory and nearby trajectories. By definition, large DLE values reveal large local sensitivity in the flow with respect to changes in initial conditions.

In numerical computations, we select a sufficiently dense grid of initial conditions for which numerical differentiation

Table 1: Parameter values, units and sources

Parameter	Value	Units
k_1	2.67×10^{-9}	cell $*$ (s $*$ molecules)$^{-1}$
k_{d1}	1×10^{-2}	s^{-1}
k_{d2}	8×10^{-3}	s^{-1}
k_3	6.8×10^{-8}	cell $*$ (s $*$ molecules)$^{-1}$
k_{d3}	5×10^{-2}	s^{-1}
k_{d4}	1×10^{-3}	s^{-1}
k_5	7×10^{-5}	cell $*$ (s $*$ molecules)$^{-1}$
k_{d5}	1.67×10^{-5}	s^{-1}
k_{d6}	1.67×10^{-4}	s^{-1}

Parameter names include the reaction number and 'd' for dissociation constants. All parameters except for k_{d5} and k_{d6} were derived from a physico-chemical model fit to quantitative data from time courses of HT-29 human colon carcinoma cells treated with TNF [Schoeberl *et al.*, unpublished results]. k_{d5} was derived using parameters in [42]. The ubiquitination rate, k_{d6}, was assumed to correlate with an average delay of 100 min between ubiquitination tagging and degradation

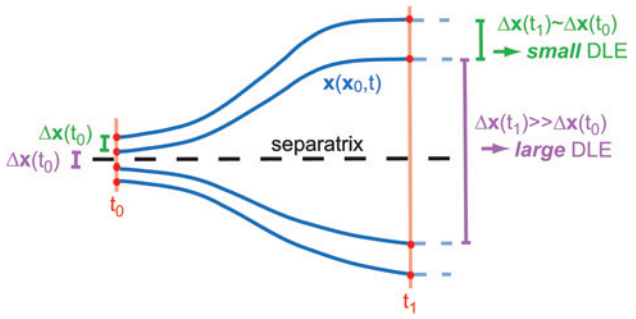

Fig. 2 *Large DLEs identify the location of maximum separation between trajectories, defining a separatrix*

DLEs measure local sensitivity to initial conditions. Relative to the time point used in the calculation of the exponent, small DLEs indicate little sensitivity (green). Large exponents indicate high sensitivity near the initial conditions (purple)

gives meaningful results. We then launch trajectories from each grid point and calculate the DLE value defined above for each trajectory. We plot the resulting DLEs over the initial grid to identify locations of highly sensitive initial conditions. Regions of phase-space exhibiting different qualitative behaviours are necessarily separated by sensitive initial conditions, and hence their boundaries (separatrices) will appear as local maximisers of the DLE field. The accuracy of separatrix locations obtained in this fashion will increase as the initial grid size is refined. By the continuous dependence of trajectories on initial conditions, separatrices are captured by our procedure even if they do not exactly intersect the initial grid. This is because separatrices have whole neighbourhoods of increased sensitivity, which are captured by a sufficiently dense initial grid.

DLEs, apart from their application described here, are particularly useful in finding repelling and attracting surfaces and have been used in fluid mechanics [40, 41] and rigid body dynamics [41]. DLEs were proved to robustly identify the locations of maximum stretching (divergence between nearby trajectories) by Haller [38, 39]. We use the maximum stretching among all dimensions to measure the rate of exponential separation for a finite-time between two neighbouring trajectories (Fig. 2).

To quantify the degree of stretching at particular initial conditions, first we define the separation (9) and approximate it by linearisation (10):

$$\begin{aligned}\boldsymbol{\zeta}(t) &= \boldsymbol{x}(t, t_0, \boldsymbol{x}_0 + \boldsymbol{\zeta}_0) - \boldsymbol{x}(t, t_0, \boldsymbol{x}_0) \\ &= \frac{\partial \boldsymbol{x}(t, t_0, \boldsymbol{x}_0)}{\partial \boldsymbol{x}_0} \boldsymbol{\zeta}_0 + O(|\boldsymbol{\zeta}_0|^2) \end{aligned} \quad (9)$$

$$\boldsymbol{\zeta}(t) \cong \frac{\partial \boldsymbol{x}(t)}{\partial \boldsymbol{x}_0} \boldsymbol{\zeta}_0 \quad (10)$$

Here $\boldsymbol{x}$ and $\boldsymbol{\zeta}$ are vectors describing species concentration and trajectory separation, respectively. Next, we define stretching as the matrix (spectral) norm of the deformation gradient $\partial \boldsymbol{x}(t)/\partial \boldsymbol{x}_0$. Recalling

$$\|\boldsymbol{A}\| = (\lambda_{\max}(\boldsymbol{A}^{\mathrm{T}}\boldsymbol{A}))^{1/2} \quad (11)$$

for a square matrix $\boldsymbol{A}$ (where $\lambda_{\max}(\boldsymbol{X})$ denotes the maximum eigenvalue of $\boldsymbol{X}$), we obtain:

$$\left\|\frac{\partial \boldsymbol{x}(t)}{\partial \boldsymbol{x}_0}\right\|^2 = \lambda_{\max}\left(\left(\frac{\partial \boldsymbol{x}(t)}{\partial \boldsymbol{x}_0}\right)^{\mathrm{T}}\left(\frac{\partial \boldsymbol{x}(t)}{\partial \boldsymbol{x}_0}\right)\right) \tag{12}$$

We then define the finite-time maximal (over all directions) stretching rate experienced along the trajectory $\boldsymbol{x}(t, t_0, \boldsymbol{x}_0)$ as:

$$\frac{1}{t-t_0}\log\left\|\frac{\partial \boldsymbol{x}(t)}{\partial \boldsymbol{x}_0}\right\| = \frac{1}{2(t-t_0)}\log\left[\lambda_{\max}\left(\left(\frac{\partial \boldsymbol{x}(t)}{\partial \boldsymbol{x}_0}\right)^{\mathrm{T}}\left(\frac{\partial \boldsymbol{x}(t)}{\partial \boldsymbol{x}_0}\right)\right)\right] \tag{13}$$

Note that we can treat $1/(2(t-t_0))$ as a constant because the stretching rates are compared at a particular time t. Therefore we can further simplify (13) to define the DLE by factoring out this constant:

$$\mathrm{DLE}(t, \boldsymbol{x}_0) = \log\left[\lambda_{\max}\left(\left(\frac{\partial \boldsymbol{x}(t)}{\partial \boldsymbol{x}_0}\right)^{\mathrm{T}}\left(\frac{\partial \boldsymbol{x}(t)}{\partial \boldsymbol{x}_0}\right)\right)\right] \tag{14}$$

2.3 DLE computation and visualisation

Classical finite-time Lyapunov exponents are typically computed for

$$\dot{\boldsymbol{x}} = \boldsymbol{f}(\boldsymbol{x}, t) \tag{15}$$

by numerically solving the linear system

$$\dot{\boldsymbol{\zeta}} = \frac{\partial \boldsymbol{f}}{\partial \boldsymbol{x}}(\boldsymbol{x}(t, t_0, \boldsymbol{x}_0), t)\boldsymbol{\zeta} \tag{16}$$

obtained from differentiating (10) in time. By contrast, DLEs are computed directly from (10), without the laborious solution of (16) along all trajectories. Specifically, we compute finite-time Lyapunov exponents directly by differentiating final trajectory positions with respect to their initial condition (hence the terminology 'direct' Lyapunov exponent).

To compute DLEs, a grid of initial conditions sampling phase-space was chosen, and each set of initial conditions was integrated with respect to time using the ode15s solver in MATLAB 7.0 (The Mathworks, Natick, Massachusetts). The deformation gradient $\partial \boldsymbol{x}(t)/\partial \boldsymbol{x}_0$ was then obtained from a numerical differentiation of final trajectory position with respect to their initial conditions. Next, the natural log of the maximum eigenvalue of the strain tensor $(\partial \boldsymbol{x}(t)/\partial \boldsymbol{x}_0)^{\mathrm{T}}(\partial \boldsymbol{x}(t)/\partial \boldsymbol{x}_0)$ was computed to find the DLE, as defined in (14), at each initial condition.

For a grid of approximately 1.6×10^6 points, the entire computation (including trajectory integration) was completed in approximately 85 h on a Linux workstation with 2 GB of memory and dual 2.80 GHz Intel Xeon processors. The points on the grid were linearly spaced along each direction. The MATLAB code performing the computation is provided at http://cdpcenter.org/. The resulting DLEs were visualised using Spotfire DecisionSite (Spotfire, Somerville, Massachusetts).

3 Results

3.1 Cell phenotypic response of apoptotic death is governed by transient signals in a caspase-mediated network

As a test case of a biologically important transient response network, we explored a mechanistic, differential equation-based model of caspase-3 activation depicted in Fig. 1. This network includes both pro-apoptotic elements (caspase-8 and caspase-3) and a pro-survival factor (XIAP). While it has only eight distinct species (and dimensions), our caspase-3 activation model is complex enough to be obscure without analysis.

In the presence of active caspase-8, this network produces a transient response that is dependent on the initial conditions (concentrations) of the eight network species (Figs. 3*a* and *b*). In cells, apoptosis is triggered by elevated and prolonged caspase-3 (or effector caspase) activation. Fig. 3 shows simulated time courses (trajectories) from our model, where apoptotic cells are categorised as exhibiting a relatively tall and wide pulse of active caspase-3, while surviving cells are characterised by short and narrow spikes of active caspase-3. As expected in a transient response system, we observe that after decay of the transient signal, pro- and anti-apoptotic time courses eventually reach the same type of steady-state (although with different concentrations of XIAP, Figs. 3*c* and *d*). A careful look at the time scale shows that it takes nearly a week for the pro-death signal to reach equilibrium. In reality, such a cell would have died before the end of two days, and this steady-state would never be reached. For simplification, this model does not include protein turnover. We observed that the introduction of turnover into our model did not significantly change its response (see online supplementary materials).

This preliminary inspection of the caspase-3 activation model demonstrates that transient signals for pro- and anti-apoptotic conditions differ qualitatively. These two types of trajectories separate from one another before reaching steady-state. Furthermore, the behaviour of the network is dependent on initial conditions. By increasing the initial concentration of XIAP, the transient signal changes from

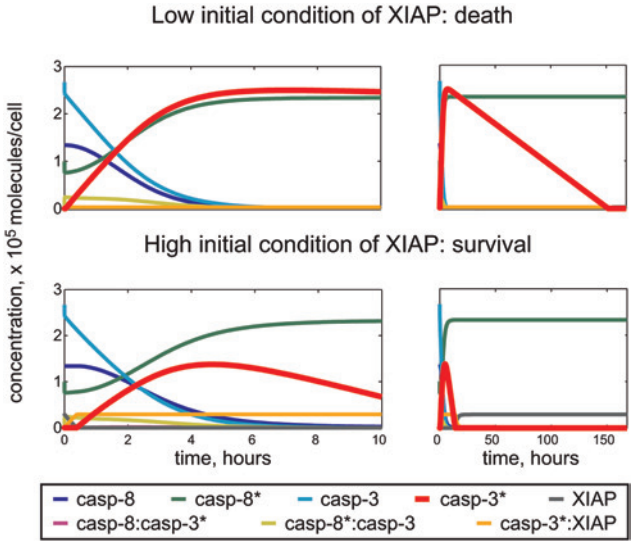

Fig. 3 *Time-course simulations show transient death and survival responses under two different initial conditions of XIAP*

a With little XIAP (2.9×10^3 molecules/cell) to inhibit activation of caspase-3, caspase-3 activation is sustained and destines this cell for death

b With more XIAP (2.9×10^4 molecules/cell), the pulse of caspase-3 activity is small and destines this cell for survival

c, *d* Longer time course shows that both apoptotic and non-apoptotic signals arrive at the same type of fixed point

The simulation conditions are the same as in *a* and *b*, respectively

In these time courses, the initial conditions were 0 molecules/cell for intermediate complexes and active caspase-3, 1×10^5 molecules/cell for active caspase-8, 1.34×10^5 molecules/cell for inactive caspase-8, and 2.67×10^5 molecules/cell for inactive caspase-3

a pro-apoptotic to a pro-survival signal (Fig. 3). We anticipate that there is a sensitive initial condition of XIAP at which the behaviour of the network changes, and that this sensitive point will shift according to initial conditions of the active and inactive caspases.

3.2 Large DLEs define a separatrix separating phase-space into pro- and anti-apoptotic regions

As described in Sections 1 and 2, we employ DLEs to search our model phase-space for regions delineating diverse behaviour of transient network signals related to different cell phenotypic responses (Fig. 2). Neighbouring trajectories in these regions will veer away from each other, thus exhibiting large DLEs that effectively define separatrices dividing the phase-space into regions possessing different trajectory behaviours. Because DLEs are calculated for the endpoint of the trajectories, they depend on the specific time point at which the trajectory separation is measured. This feature is a crucial aid in studying transient response systems, for it insures that the analysis can be performed on the basis of transient signals.

To characterise the network's dependence on initial conditions in multiple dimensions, we computed DLEs across an eight-dimensional grid spanning a wide range of initial species concentrations. Totalling approximately 1.6×10^6 points, the grid points are linearly spaced along each direction. These concentrations were chosen to encompass protein expression across cell populations and under different signalling conditions in Hct-116, HeLa and HT-29 carcinoma cell lines (10^2–10^5 molecules/cell for XIAP and $10^2 - 3.5 \times 10^6$ molecules/cell for the caspases [S. Gaudet and K. Leitermann, personal communication]). Biochemical intermediates were sampled with coarser resolution because they were not found to contribute to the network behaviour (data not shown). To find a separatrix, DLEs were calculated at 6 h, by which time Hct-116, HT-29 and HeLa cells would have responded to treatment with death-inducing ligands tumor necrosis factor (TNF) or TNF-related apoptosis-inducing ligand (TRAIL) [Aldridge *et al.*, unpublished observations]. To determine how narrow the time window of effective separatrix appearance might be, we additionally undertook DLE calculations across the range between 2 and 12 h, and found that the separatrix did not move noticeably (data not shown).

As it is problematic to simultaneously visualise the phase space in eight-dimensions, in Fig. 4 we offer more accessible illustrations of the DLEs in three-dimensional slices. Fig. 4*a* illustrates the DLEs in the subspace containing XIAP, caspase-8 and active caspase-8, whereas Fig. 4*b* shows the DLEs in the subspace containing XIAP, active caspase-8 and active caspase-3. Large DLEs (blue) define a finite-time separatrix that identifies the points at which the balance between XIAP and active caspase-8 shifts so that the overall response changes from pro-apoptotic to anti-apoptotic signals. We expected the apoptosis regulatory network to have a separatrix because the cell's response is either survival or death – it is not graded (from alive to sick to dead). If a system were to exhibit a more graded response, the DLEs would have been more uniform across phase-space and would not have yielded a discernible separatrix.

The location and shape of the separatrix provide a framework to generate conceptual interpretation of network operation. The separatrix shifts towards higher XIAP concentrations as the amount of active caspase-8 increases

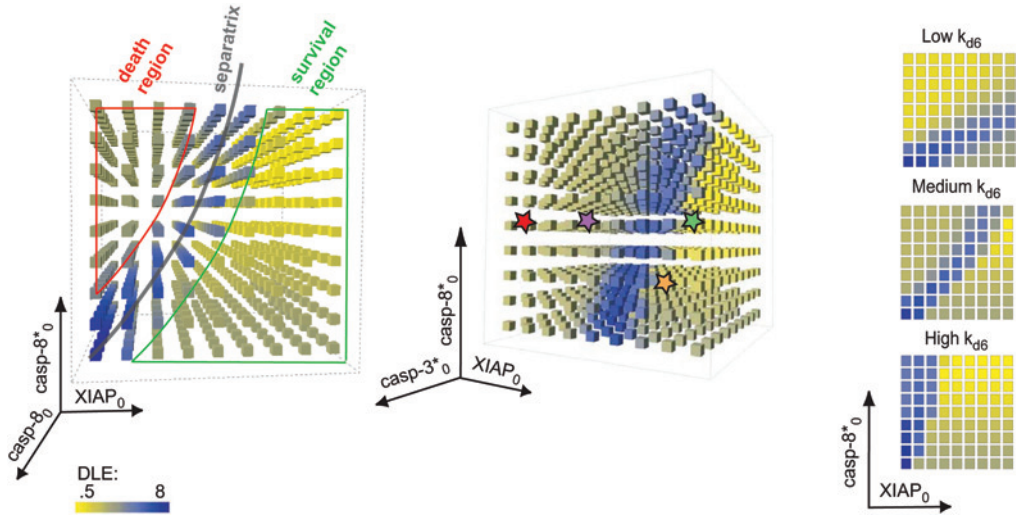

Fig. 4 *Six-hour DLE defines a separatrix separating phase-space into pro- and anti-apoptotic decisions*

Phase-space subplots are shown on a linear scale with initial conditions of XIAP and the active caspases ranging from 1×10^2 to 1×10^5, and 1×10^2 to 3.5×10^5 molecules/cell for the inactive caspases. All concentrations refer to initial conditions. The subspaces plotted were chosen to closely match the protein concentrations in untreated HT-29 cells [S. Gaudet and K. Leitermann, personal communication]

a, *b* Large DLEs of the caspase-3 activation network at six hours define a separatrix. The blue curve is the separatrix which divides the phase-space into regions where cells survive (to the right of the separatrix) or die (to the left of the separatrix)

a DLEs are shown in a subspace containing XIAP, active caspase-8, and inactive caspase-8 with 2.6×10^5 molecules/cell of inactive caspase-3 and 1×10^2 molecules/cell of active caspase-3 and the intermediate complexes. The gray curve highlights the separatrix, while the pro- and anti-apoptotic regions are outlined in red and green, respectively

b DLEs are shown in the subspace containing XIAP, active caspase-8, and active caspase-3 with 2.6×10^5 molecules/cell of inactive caspase-3 and inactive caspase-8, and 1×10^2 molecules/cell of the intermediate complexes. The stars indicate reference points (individual cells with different protein levels). The red and purple cells are pro-apoptotic while the green and orange cells are anti-apoptotic

c Separatrix shape is sensitive to rate constants. As the rate of ubiquitination is decreased (k_{d6} increased), the slope of the separatrix increases. The DLEs are shown in the subspace containing XIAP and active caspase-8, with 2.6×10^5 molecules/cell of inactive caspase-3 and inactive caspase-8, and 1×10^2 molecules/cell of the intermediate complexes and active caspase-3. From low to high, the rate constant k_{d6} has values 3.33×10^{-5}, 1.67×10^{-4} and 8.3×10^{-4} s^{-1}

(Fig. 4*a*). Cells will die if above the separatrix, whereas below the separatrix there is enough XIAP to overcome the conversion of inactive caspase-3 to active caspase-3 by active caspase-8. The separatrix shape is invariant to inactive caspase-8, suggesting that the positive feedback activating caspase-8 by caspase-3 has less influence than the regulation of caspase-3 by active caspase-8 and XIAP. As XIAP tags active caspase-3 for degradation, more XIAP would be needed to rescue the cell from a death decision if there was a higher initial concentration of active caspase-3 (Fig. 4*b*). Fig. 4*c* shows perturbations to the separatrix as the ubiquitination rate constant is changed. As the rate increases, so does the slope of the separatrix in the XIAP and active caspase-8 subspace. The slower the ubiquitination rate, the longer the complex of active caspase-3 and XIAP will exist, effectively lowering the concentration of free XIAP. We also observed that the separatrix is not a simple plane – it curves at higher concentrations of active caspase-8 and shifts slope as the ubiquitination rate changes (Fig. 4*c*).

In addition to using the separatrix as a tool to help us interpret the decision-making mechanisms of the network, the separatrix quantitatively identifies the critical ratios of initial conditions around which the cell response changes. By comparing the location of different cells in phase space to each other and the separatrix, we can evaluate how differences in species concentrations affect differential cell behaviour. It is informative to note that the location of a cell in phase- or concentration-space affects how the network reacts to signals. For example, consider two cells in the pro-apoptotic section of phase-space that have different XIAP concentrations (as indicated in Fig. 4*b*). The purple and red starred cells are close to and far from the separatrix, respectively. The red starred cell requires an eight-fold increase in XIAP concentration to cross the separatrix (to reach the green) while the purple starred cell needs a modest two-fold increase. Alternatively, the red starred cell could move to the separatrix by increasing its XIAP concentration six-fold while decreasing its active caspase-8 concentration by one half (orange star). If the XIAP concentration is increased four-fold in both cells, the cells will behave differently and only the purple starred cell will cross the separatrix to survive. This simple example illustrates that we need to know the cell's state (key species concentrations) before predicting response. The DLE-defined separatrix helps us understand how cells in different states can have disparate responses to the same stimulation or perturbation.

3.3 Steady-state analysis cannot distinguish pro- and anti-apoptotic responses across phase-space

Direct analysis of the set of nonlinear algebraic equations representing our model at steady-state showed that the system has four types of equilibria (that is, four invariant manifolds filled with fixed points, in contrast to four fixed points) with only one type being stable (Fig. 5*a*, online supplementary materials). These stable fixed points can have non-zero valued concentrations of caspase-8 and XIAP. However, the concentration of caspase-3 must be zero because any inactive caspase-3 would be activated by caspase-8 and subsequently degraded by XIAP before a steady-state is reached. The phase-space locations of these stable fixed points are dependent on initial conditions.

To investigate whether these stable steady-states segregate into pro- and anti-apoptotic clusters, we plotted the steady-state locations from small subsets of trajectories. Figs. 5*b*–*d* show active and inactive caspase-8 equilibrium concentrations from different small sets of trajectories.

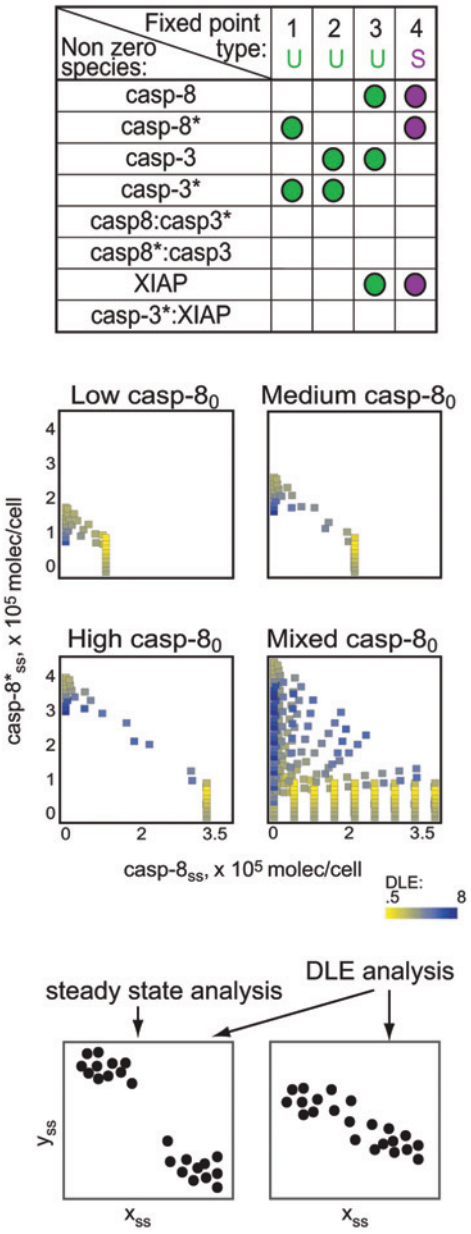

Fig. 5 *Stability and steady-state analyses of the caspase-3 activation network model*

a Stability analysis shows one stable (purple) and three unstable (green) types of fixed points (see online supplementary materials). Every type of fixed point requires concentrations of zero for the intermediate complexes. For each of the four fixed point types, there are two or three species that can be nonzero. Green (unstable) and purple (stable) circles indicate which species can be nonzero for each type of fixed point.

b–*e* Steady-state locations in the caspase-3 activation network are not globally clustered. Fixed points are plotted in the subspace containing active and inactive caspase-8, with increasing initial concentrations of inactive caspase-8: *b* 8.8×10^4, *c* 18×10^5 and *d* 3.5×10^5 molecules/cell. Other initial conditions were 2.6×10^5 molecules/cell of inactive caspase-3, 1×10^2 molecules/cell of active caspase-3 and the intermediate complexes, and 1×10^2–1×10^5 molecules/cell for active caspase-8 and XIAP. For each initial concentration of inactive caspase-8 (*b*–*d*), the steady-states are moderately clustered and are segregated by large DLEs (blue). However, the fixed points from different inactive caspase-8 initial conditions do not cluster when plotted together (*e*)

f Schematic compares the use of steady-state and DLE analysis methods. In systems where steady-states localise to different regions of phase space (left), steady-state analysis methods may be used to characterise the phenotypic behaviour of the network. DLE analysis can distinguish between behaviours in networks regardless of fixed point clustering

Within each set, the initial conditions of inactive caspase-8 were constant and most steady-states cluster into death or survival locales. For example, cells that survive stimulation with a death stimulus generally have low active and high inactive caspase-8 concentrations because caspase-3 was not activated enough to convert most of the inactive caspase-8 to the active form. This suggests that within a small set of initial conditions, a separatrix can be identified by plotting stable fixed points.

However, when we plotted trajectories from a broader range of initial concentrations of caspase-8, the ability to distinguish cell fate based on steady-state locations is lost (Fig. 5*e*). In contrast, DLEs can separate the two fates without considering steady-state values. We have seen in Fig. 4 that large DLEs can define a separatrix over a broad set of initial conditions. For the small sets described above, equilibria between the clusters have large DLEs and separate the groups representing surviving and dying cells (Figs. 5*b*–*d*). We conclude that DLEs are versatile and can be applied regardless of whether or not steady-states cluster by behaviour (Fig. 5*f*).

4 Discussion

Our goal here is to develop an analysis methodology for differential equation models aimed at understanding how transient signals influence phenotypic responses, that is, to develop signal-response relationships for most transient response networks in higher cells. Many signal transduction networks are transient response networks, meaning that they affect phenotypic cell responses before a steady-state is reached. Therefore the steady-state and bifurcation analysis methods traditionally used to study differential equation-based models do not find straightforward application to transient response networks. To successfully analyse complex networks, we required that our methodology be applicable to transient signals across multiple dimensions.

Towards this challenging goal, we have described the use of DLEs to study differential equation models of transient response networks. DLEs measure the separation between initially nearby trajectories in phase-space. We have used DLEs to identify sensitive regions of phase-space where small changes in the initial concentrations of network species alter cell fate (Fig. 2). The separation can be calculated at any specific point in time, permitting prior biological knowledge concerning the most relevant experimental measurements to be leveraged. DLEs enable an exhaustive, multi-dimensional analysis of transient signals because they measure trajectory separation with respect to each dimension across the entire phase-space. As a result, DLEs are capable of identifying both important network interactions and in what context they affect signalling (that is, at what time or under which sets of initial conditions). By searching phase-space for sensitive initial conditions (those with large DLEs), we can identify surfaces (separatrices) that separate different classes of signals. A separatrix specifies critical combinations of species concentrations around which signalling changes qualitatively. Because we can visualise the separatrix in different regions of phase-space, DLE analysis enables us to quantitatively interpret complex signalling interactions.

In applying DLE analysis to other biological signalling networks, a few considerations must be explored. DLE analysis is a numerical method which is flexible in the grid resolution and finite-times chosen for evaluation. While this flexibility is an asset for studying biological systems which have different time scales and varying parameter sensitivities, crude choices of time and phase-space grid may not capture all separatrices of interest. Because of the continuous dependence of trajectories on initial conditions, however, the DLE computation is a convergent procedure: refined grids and longer integration times are guaranteed to capture all separatrices. A second consideration is the relative strength of rates at which trajectories diverge at different locations in phase-space. Large rates of divergence will dominate the calculations, possibly obscuring smaller but biologically important trajectory separations. Therefore it is important to select visualisation methods that identify local features of the DLE field efficiently, thereby ensuring that all key behaviours are illuminated.

As a particular example of current biological interest, we applied DLE analysis to a model of caspase-3 activation involving caspase-8 and XIAP. The model responds to a pro-death stimulus with a transient signal leading to either death or survival. This network is an example of a transient response network: it has only one type of stable steady-state and the survival against death decision is made before this steady-state is reached. Because caspase-3 cleaves its substrates irreversibly, key cell components will be degraded before caspase-3 activity reaches steady-state. This notion of transient response signalling in apoptosis differs from some previously published models, which have cast this phenomenon as a multiple steady-state problem and analysed it accordingly [29, 30]. Although some insights concerning model parameter effects were gained in those contributions, recent experimental studies focused on dynamic and integrative measurement have demonstrated that the key signals governing the phenotypic outcome of cell death against survival are transient [28, 31]. Before stimulation, this network rests at a basal steady-state. Upon stimulation, a transient signal is produced during which the life against death outcome is decided. Cells that survive return to the basal state. Thus, all key physiological signalling occurs during the transient phase.

While our model describes only a subset of the complex network regulating caspase-3, the model has eight species and is too complex to be comprehensively characterised by inspection or parameter sensitivity analysis. Because DLE analysis is time-dependent and multivariate, we were able to gain specific insights about the regulation of caspase-3 that most likely would have been overlooked by inspection, single-parameter sensitivity analysis, or steady-state analysis (Fig. 5*f*). Large DLEs defined a separatrix, from which we were able to gain quantitative, multivariate insight into the death against survival decision. The separatrix classified two types of transient signals and defined the conditions leading to apoptosis and survival (Fig. 4). We observed that the shape of the separatrix is not a simple plane and its shape and slope are dependent on rate constants. This suggests that in cases where reactions rates are hard to measure, the constant could be fit by comparing an experimentally identified separatrix with computationally predicted separatrices.

We envision DLE analysis as a tool for addressing challenging practical problems such as understanding the role of cell population heterogeneity in disease diagnosis and treatment. Others have described how population averages differ from the behaviour of single cells by using population heterogeneity [18, 29]. DLE analysis can be used to investigate a key tangential question: How does population heterogeneity of protein expression correlate with different single-cell behaviours in a population of cells? To study the effects of noise and variability in protein expression within a population of cells, we can compare the concentration distributions of key proteins with separatrices. Intersections between these distributions and separatrices should correlate with heterogeneous responses. For

example, when cells are treated with a saturating concentration of TNF, a death-inducing ligand, only approximately 60% of a population of HT-29 cells die [28]. While not understood in quantitative terms, the TNF receptor is known to activate both pro-survival and pro-apoptotic pathways. The pre-death inducing signalling complex activates the nuclear factor-κB (NF-κB) pathway (a pro-survival pathway that upregulates XIAP) before activating caspase-8 and the mitochondrial pathway. Activation of the mitochondrial pathway causes the mitochondria to release Smac, a pro-apoptotic protein which inhibits XIAP. It is likely that within a cell population, basal protein expression variation can affect network behaviour by changing the concentrations of key regulatory proteins such as XIAP. In the future, the phase-space locations of HT-29 cells could be determined experimentally by measuring the distribution of caspase-3, caspase-8 and XIAP expression levels. By evaluating their proximities to the separatrix, we could determine if the distribution of protein expression levels in a cell population can cause a heterogeneous response to TNF treatment. Eventually, we anticipate that DLE analysis can help us understand the transformation of a cell from a healthy to diseased state, and identify what changes in species concentrations are required to move the diseased cell across the separatrix to a healthier condition.

5 Acknowledgments

The authors thank Suzanne Gaudet, John Albeck, John Burke, Sampsa Hautaniemi, Robert Szalai and Laura Sontag for stimulating and helpful discussions. This work was supported by the NIGMS Cell Decision Processes Center grant (P50-GM68762) to PKS and DAL, and a US Department of Energy Computational Science Graduate Fellowship to BBA.

6 References

1 Huang, C.Y., and Ferrell, J.E. Jr.: 'Ultrasensitivity in the mitogen-activated protein kinase cascade', *Proc. Natl. Acad. Sci. USA*, 1996, **93**, (19), pp. 10078–10083
2 Kholodenko, B.N., *et al.*: 'Quantification of short term signalling by the epidermal growth factor receptor', *J. Biol. Chem.*, 1999, **274**, (42), pp. 30169–30181
3 Bhalla, U.S., and Iyengar, R.: 'Functional modules in biological signalling networks'. Novartis Found Symp., 2001, vol. 239, pp. 4–13; discussion pp. 13–5, 45–51
4 Schoeberl, B., *et al.*: 'Computational modeling of the dynamics of the MAP kinase cascade activated by surface and internalized EGF receptors', *Nat. Biotechnol.*, 2002, **20**, (4), pp. 370–375
5 Novak, B., and Tyson, J.J.: 'Modelling the controls of the eukaryotic cell cycle', *Biochem. Soc. Trans.*, 2003, **31**, (6), pp. 1526–1529
6 Bhalla, U.S.: 'Models of cell signalling pathways', *Curr. Opin. Genet. Dev.*, 2004, **14**, (4), pp. 375–381
7 Nelson, D.E., *et al.*: 'Oscillations in NF-κB signaling control the dynamics of gene expression', *Science*, 2004, **306**, (5696), pp. 704–708
8 Davidson, E.H., *et al.*: 'A provisional regulatory gene network for specification of endomesoderm in the sea urchin embryo', *Dev. Biol.*, 2002, **246**, (1), pp. 162–190
9 Kitano, H.: 'Systems biology: a brief overview', *Science*, 2002, **295**, (5560), pp. 1662–1664
10 Hornberg, J.J., *et al.*: 'Control of MAPK signalling: from complexity to what really matters', *Oncogene*, 2005, **24**, (36), pp. 5533–5542
11 Thattai, M., and van Oudenaarden, A.: 'Attenuation of noise in ultrasensitive signalling cascades', *Biophys. J.*, 2002, **82**, (6), pp. 2943–2950
12 Rosenfeld, N., *et al.*: 'Gene regulation at the single-cell level', *Science*, 2005, **307**, (5717), pp. 1962–1965
13 Lidstrom, M.E., and Meldrum, D.R.: 'Life-on-a-chip', *Nat. Rev. Microbiol.*, 2003, **1**, (2), pp. 158–164
14 Chong, H., Vikis, H.G., and Guan, K.L.: 'Mechanisms of regulating the Raf kinase family', *Cell. Signal.*, 2003, **15**, (5), pp. 463–469
15 Tyson, J.J., Chen, K.C., and Novak, B.: 'Sniffers, buzzers, toggles and blinkers: dynamics of regulatory and signalling pathways in the cell', *Curr. Opin. Cell Biol.*, 2003, **15**, (2), pp. 221–231
16 Resat, H., *et al.*: 'An integrated model of epidermal growth factor receptor trafficking and signal transduction', *Biophys. J.*, 2003, **85**, (2), pp. 730–743
17 Hatakeyama, M., *et al.*: 'A computational model on the modulation of mitogen-activated protein kinase (MAPK) and Akt pathways in heregulin-induced ErbB signalling', *Biochem. J.*, 2003, **373**, (2), pp. 451–463
18 Hua, F., *et al.*: 'Effects of Bcl-2 levels on Fas signalling-induced caspase-3 activation: molecular genetic tests of computational model predictions', *J. Immunol.*, 2005, **175**, (2), pp. 985–995
19 Sasagawa, S., *et al.*: 'Prediction and validation of the distinct dynamics of transient and sustained ERK activation', *Natl. Cell Biol.*, 2005, **7**, (4), pp. 365–373
20 Bhalla, U.S., Ram, P.T., and Iyengar, R.: 'MAP kinase phosphatase as a locus of flexibility in a mitogen-activated protein kinase signalling network', *Science*, 2002, **297**, (5583), pp. 1018–1023
21 Lauffenburger, D.A.: 'Cell signalling pathways as control modules: complexity for simplicity?', *Proc. Natl. Acad. Sci. USA*, 2000, **97**, (10), pp. 5031–5033
22 Swameye, I., *et al.*: 'Identification of nucleocytoplasmic cycling as a remote sensor in cellular signalling by databased modeling', *Proc. Natl. Acad. Sci. USA*, 2003, **100**, (3), pp. 1028–1033
23 Bentele, M., *et al.*: 'Mathematical modeling reveals threshold mechanism in CD95-induced apoptosis', *J. Cell. Biol.*, 2004, **166**, (6), pp. 839–851
24 Mendes, P., and Kell, D.: 'Non-linear optimization of biochemical pathways: applications to metabolic engineering and parameter estimation', *Bioinformatics*, 1998, **14**, (10), pp. 869–883
25 Markevich, N.I., Hoek, J.B., and Kholodenko, B.N.: 'Signaling switches and bistability arising from multisite phosphorylation in protein kinase cascades', *J. Cell Biol.*, 2004, **164**, (3), pp. 353–359
26 Tyson, J.J., Csikasz-Nagy, A., and Novak, B.: 'The dynamics of cell cycle regulation', *Bioessays*, 2002, **24**, (12), pp. 1095–1109
27 Pomerening, J.R., Kim, S.Y., and Ferrell, J.E. Jr.: 'Systems-level dissection of the cell-cycle oscillator: bypassing positive feedback produces damped oscillations', *Cell*, 2005, **122**, (4), pp. 565–578
28 Gaudet, S., *et al.*: 'A compendium of signals and responses triggered by prodeath and prosurvival cytokines', *Mol. Cell. Proteomics*, 2005, **4**, (10), pp. 1569–1590
29 Eissing, T., *et al.*: 'Bistability analyses of a caspase activation model for receptor-induced apoptosis', *J. Biol. Chem.*, 2004, **279**, (35), pp. 36892–36897
30 Bagci, E.Z., *et al.*: 'Bistability in apoptosis: roles of Bax, Bcl-2 and mitochondrial permeability transition pores', *Biophys. J.*, 2006, **90**, (5), pp. 1546–1559
31 Janes, K.A., *et al.*: 'A systems model of signalling identifies a molecular basis set for cytokine-induced apoptosis', *Science*, 2005, **310**, (5754), pp. 1646–1653
32 Hengartner, M.O.: 'The biochemistry of apoptosis', *Nature*, 2000, **407**, (6805), pp. 770–776
33 Danial, N.N., and Korsmeyer, S.J.: 'Cell death: critical control points', *Cell*, 2004, **116**, (2), pp. 205–219
34 Shi, Y.: 'Mechanisms of caspase activation and inhibition during apoptosis', *Mol. Cell.*, 2002, **9**, (3), pp. 459–470
35 Boatright, K.M., *et al.*: 'A unified model for apical caspase activation', *Mol. Cell.*, 2003, **11**, (2), pp. 529–541
36 Suzuki, Y., *et al.*: 'X-linked inhibitor of apoptosis protein (XIAP) inhibits caspase-3 and -7 in distinct modes', *J. Biol. Chem.*, 2001, **276**, (29), pp. 27058–27063
37 Salvesen, G.S., and Duckett, C.S.: 'IAP proteins: blocking the road to death's door', *Natl. Rev. Mol. Cell Biol.*, 2002, **3**, (6), pp. 401–410
38 Haller, G.: 'Distinguished material surfaces and coherent structures in three-dimensional fluid flows', *Phys. D*, 2001, **149**, (4), pp. 248–277
39 Haller, G.: 'Lagrangian coherent structures from approximate velocity data', *Phys. Fluids*, 2002, **14**, (6), pp. 1851–1861
40 Wang, Y., *et al.*: 'Closed-loop Lagrangian separation control in a bluff body shear flow model', *Phys. Fluids*, 2003, **15**, (8), pp. 2251–2266
41 El Rifai, K., Bajaj, A.K., and Haller, G.: 'Global dynamics of an autoparametric spring-mass-pendulum system and rigid body dynamics', *Nonlinear Dyn.*, 2005, unpublished
42 Deveraux, Q.L., *et al.*: 'Cleavage of human inhibitor of apoptosis protein XIAP results in fragments with distinct specificities for caspases', *Embo. J.*, 1999, **18**, (19), pp. 5242–5251